12TH INTERNATIONAL SYMPOSIUM ON FLOW VISUALIZATION
September 10-14, 2006, German Aerospace Center (DLR), Göttingen, Germany
doi: 10.5281/zenodo.14846

AN OPTICAL FLOW BASED TECHNIQUE FOR THE NON-INVASIVE MEASUREMENT OF MICROFLUIDIC FLOWS

Christoph Garbe[1] , **Karsten Roetmamm**[2] , **Bernd Jähne**[1]
[1]**Interdisciplinary Center for Scientific Computing (IWR), Univ. Heidelberg, Germany;**
[2]**Laser-Laboratorium Göttingen e.V., Göttingen, Germany**

Keywords: *Optical Flow, Microfluidic, Molecular Tagging Velocimetry*

ABSTRACT

A new approach for estimating motion in microfluidic flows is presented. Is is based on an extension of the brightness changes constraint equation (BCCE) to incorporate Taylor dispersion. This extended BCCE is then used for accurately estimating fluid flows in a two dimensional Molecular Tagging Velocimetry (2D-MTV) framework. Reference measurements were conducted to validate the accuracy and applicability of the novel technique. Due to the excellent agreement between measurement and ground truth, the method was also applied to inhomogeneous flows in a mixing chamber.

1 INTRODUCTION

In recent years, the area of microfluics has expanded tremendously. Technological progress in manufacturing microfluid components has lead to a spread of novel systems into diverse applications [1, 2, 15, 22, 3]. In chemical and biochemical analytics as well as in medical diagnostics, these novel devices can be used to speed up the analysis while only relying on minute probe volumes. This is due to the huge surface to volume ratio achievable by micro channels. In the future, microfluidic applications will increase in significance for chemical production processes. Here, boundary conditions can be controlled much more accurately and set accordingly. This leads to better controllable and thus more efficient reaction kinetics with less by-products.

This increase of interest in microfluidic devices directly leads to the need for diagnostic tools for the visualization, analysis of flow structures, mixture formation and reaction behavior directly inside the micro channels[18]. Here, non destructive image-driven methods are preferable for various reasons.

In the presented contribution, an optical flow based technique will be presented that allows estimating the motion of micfofluidic flows visualized through molecular tagging with a special dye.

2 EXPERIMENTAL SET-UP

The technique for measuring flow velocities of microfluidic flows presented in this contribution relies on caged dyes as markers in the flow. The reader is referred to [16] for a detailed description of the set-up and dyes used.

Basically, the microfluidic flows are measured in a specially prepared camber. Two glass plates are separated by $2d = 250\mu$m. In order to visualize the fluid flow, markers or tags have to be affixed to the flow. Obviously, the markers should not change the flow itself or introduce additional flow components. A very elegant way of introducing these markers is through the use of dyes. The dyes do not change the density of the fluid significantly as the dye molecules stick to the water molecules. Hence, no additional flow components are introduced by buoyancy or electrostatic properties in the same way particles of PIV applications would.

The set-up and visualization process leads to the following procedure: at time $t_0 = 0$ the intensity structures are written with the XeF Laser into the fluid. The fluid inside the chamber is accessible non-invasively only through the glass plates on top and bottom of the Poiseuille flow. The beam of the laser writing the structured to the flow thus traverses through the whole depth of the fluid. A circular dot in the mask written to the fluid will thus appear as a cylinder in the flow structure. In later times, this 3D cylinder is sheared by the paraboloid velocity profile developed by the Poiseuille flow. The 2D cut of this process is shown for three time steps t_1-t_3 in Figure 1**a** . These transformed 3D Structures are projected onto the CCD chip of the imaging device. Great care is taken to align the camera orthogonal to the glass plate. Through this projection, it appears as if the structure written to the fluid is smeared in the direction of the fluid flow over time. This process is also known as *Taylor dispersion* [19].

3 TAYLOR DISPERSION

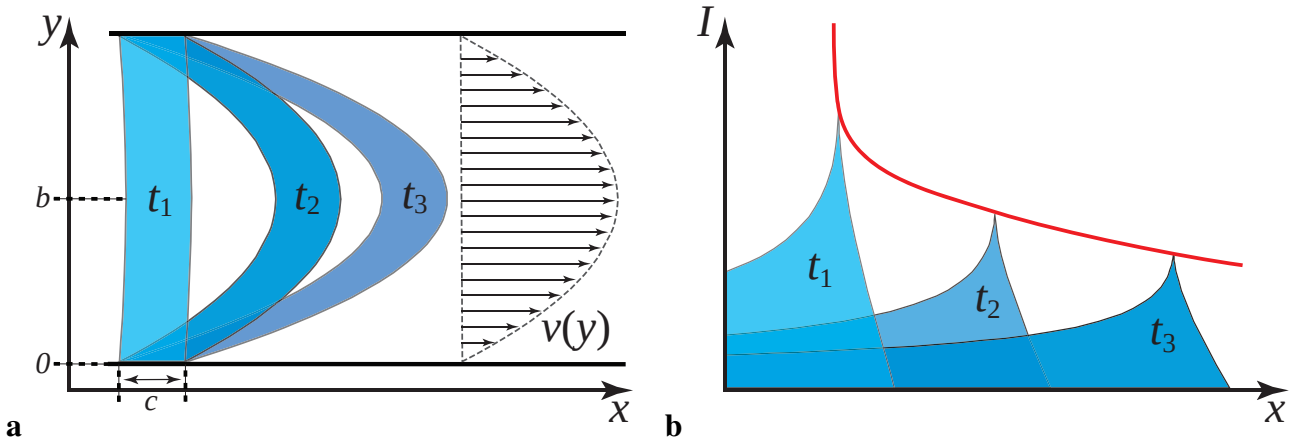

Fig. 1 A sketch of the intensity profile of the dye for a Poiseuille flow at three times t_1-t_3 is shown in **a** together with the velocity profile $v(y)$. The projection of these profiles onto one plate as seen by the camera is shown in **b** .

A viscous fluid driven by a pressure gradient in between two stationary plates is also known as plane Poiseuille flow in the case of purely laminar flows[12]. In the present application of microfluidic flows, the Reynolds number Re is in well within the laminar limit. The velocity profile of a Poiseuille flow is given by

$$v(y) = \frac{a}{2}y^2 - a \cdot b \cdot y \quad \text{with} \quad a = \frac{1}{\mu}\frac{dP}{dx}, \tag{1}$$

where $2b$ is the separation of the stationary plates, μ is the viscosity of the fluid and dP/dx is the pressure gradient along the direction of the flow. The flow and the associated quantities are visualized in the sketch of Figure 1 **a** .

The maximum velocity $v_{\max}$ of the flow is given at the center in between the two plates at $x = b$. This velocity is thus given by

$$v_{\max} = v(b) = -\frac{a}{2} \cdot b^2. \tag{2}$$

The fluid inside the chamber is accessible non-invasively only through the glass plates on top and bottom of the Poiseuille flow. Three dimensional intensity structures are thus projected onto these plates and visualized. As pointed out in Section 2, a three dimensional structures can be written to the fluid with a masked laser beam. The beam of the laser writing the structured to the flow traverses through the whole depth of the fluid confined between the two plates. A circular dot in the mask will thus appear as a cylinder in the flow structure. In later times, this 3D cylinder is sheared by the paraboloid velocity profile given by Equation (1). The 2D cut of this process is shown for three time steps t_1-t_3 in Figure 1**a** . Through this projection, it appears as though the structure written to the fluid is smeared in the direction of the fluid flow over time.

The projection of the dye intensity onto the glass plates by the imaging process is then given by integrating the intensities over the depth in between the plates. This results in

$$I = \sqrt{\left\| b^2 + \frac{2 \cdot (c+x)}{a \cdot t} \right\|} - \sqrt{\left\| b^2 + \frac{2 \cdot x}{a \cdot t} \right\|}. \tag{3}$$

This analytic function is visualized in the sketch in Figure 1**b** .

The maximum of the projected intensity is given by

$$I_{\max} = \sqrt{\left\| \frac{2 \cdot c}{a \cdot t} \right\|}. \tag{4}$$

The location of this intensity maximum $x_{\max}$ can be found to be

$$x_{\max} = -\frac{a}{2} \cdot b^2 \cdot t \tag{5}$$

and subsequently the velocity of the intensity maximum to

$$v_{\max} = \frac{\partial x_{\max}}{\partial t} = -\frac{a}{2} \cdot b^2. \tag{6}$$

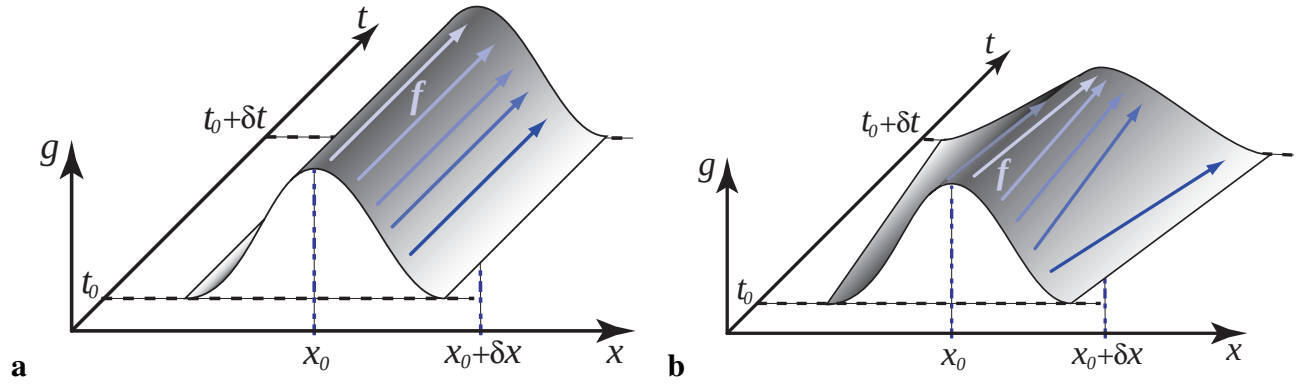

Fig. 2 Illustration of the brightness change constraint equation. A one dimensional grey value distribution is moved along the x-axis. In **a** constant brightness is assumed. During the translation from point x_0 to $x_0 + \delta x$ the grey value distribution stays the same over the period δt. This can be formulated as $dg/dt = 0$. In **b** the grey value distribution is changed according to a diffusion process. The BCCE estimates the optical flow incorrectly.

By comparing this equation with the expression of the maximum velocity from the velocity profile in Equation (2) it becomes apparent, that the velocity of the intensity maximum is equivalent to the velocity halfway in between the two plates. This result is not surprising, as the intensity maximum of the projection is collocated to the trailing edge of the written structures halfway in between the plates. This can easily be seen in Figure 1.

This would open up the possibility of measuring $v_{\max}$ by tracking the intensity peak of the projected intensity distribution. However, finding this peak to a subpixel accuracy can be quite challenging. Fitting Equation (3) to the measured greyvalue distribution would implicitly assume that the velocity profile is stationary and does not change in time. This is too strong a limitation, since we are interested in measuring time-dependent flows. For this reason, a local gradient based technique for measuring velocities from image sequences was chosen for this work. The algorithm and results shall be presented in the following.

4 OPTICAL FLOW COMPUTATIONS

The technique of simultaneously estimating optical flow and change of image intensity is well known in literature [14, 23, 10, 9]. Details of the technique employed in the context of this paper, including the estimation of local convergence and divergence, have been explained previously [6]. Accuracy improvements were introduced in [5] and [7]. Therefore, only a brief overview of the technique shall be presented here.

A very common assumption in optical flow computations is the brightness change constraint equation (BCCE) [11]. It is assumed that the image brightness of a scene point remains constant in a spatio-temporal neighborhood. That is the image intensity g at the location (x,y) at time t stays the same in a time interval ∂t during which a translation by $(\partial x, \partial y)$ took place. This brightness constancy model can

be formulated as

$$g\,(x+\partial x, y+\partial y, t+\partial t) = g\,(x,y,t)\,. \tag{7}$$

Developing this equation up to first order in a Taylor series expansion leads to

$$g\,(x+\partial x, y+\partial y, t+\partial t) = g(x,y,t) + \frac{\partial g}{\partial x}\frac{\mathrm{d}x}{\mathrm{d}t}\partial t + \frac{\partial g}{\partial y}\frac{\mathrm{d}y}{\mathrm{d}t}\partial t + \frac{\partial g}{\partial t}\partial t + O(\mathbf{f}^2). \tag{8}$$

The well known brightness change constraint Equation (BCCE) [4, 11] is then derived by simplifying Equation (8) and differentiating by ∂t, thus

$$\frac{dg}{dt} = \frac{\partial g}{\partial t} + \frac{\partial g}{\partial x}\frac{\mathrm{d}x}{\mathrm{d}t} + \frac{\partial g}{\partial y}\frac{\mathrm{d}y}{\mathrm{d}t} = g_t + (\mathbf{f}\nabla)g = 0. \tag{9}$$

With the optical flow $\mathbf{f} = (dx/dt, dy/dt)^\top = (u,v)^\top$, the spatial gradient ∇g and the partial time derivative $g_t = \partial g/\partial t$. This formulation of the BCCE states that the image brightness $g(\mathbf{x},t)$ at the location $\mathbf{x} = (x_1,x_2)^\top$ should change only due to motion, that is, the total derivative of its brightness has to vanish, which is illustrated in Figure 2. [17] and [21] proved that this assumption holds provided that no illumination changes are present and the surface of the object are Lambertian in nature.

Clearly this assumption does not hold in most scientific applications. Depending on the visualization technique used, brightness changes may occur due to changes in densities. For example, due to isotropic diffusion the images substance will decrease in brightness according to the diffusion process. Obviously this brightness change is not connected to any motion, thus violating the assumption for deriving Equation (9). This effect is illustrated in Figure 2. Here iso-brightness lines are not corresponding to the movement any more. To accommodate this fact an extension to the used conservation law has to be formulated. The use of a linear model with a multiplier and offset term has been suggested [13]. Here we follow [10, 8, 6] in reformulating Equation (9) as a linear partial differential equation.

The brightness of a moving pattern is allowed to change according to an analytical function h, that is

$$g(\mathbf{x}) = h(g'(\mathbf{x}),\mathbf{b}), \quad \text{and} \quad g'(\mathbf{x}) = h^{-1}(g(\mathbf{x}),\mathbf{b}), \tag{10}$$

where $h(g(\mathbf{x}),\mathbf{b})$ is a scalar invertible transformation with the q-dimensional parameter vector $\mathbf{b} = (b_1,\ldots,b_q)^\top$ and the identity element $h(g(\mathbf{x}),0) = g(\mathbf{x})$. The total derivative of Equation (10) is then given by

$$g_t + (\mathbf{f}\nabla)g = f(g'(\mathbf{x}),\mathbf{b}) \tag{11}$$

with

$$f(g'(\mathbf{x}),\mathbf{b}) = \frac{d}{dt}h(g'(\mathbf{x}),\mathbf{b}). \tag{12}$$

For the special case of constant brightness $(h(g'(\mathbf{x}),\mathbf{b}) = \text{const} \Rightarrow f(g'(\mathbf{x}),\mathbf{b}) = 0)$ this equation reduces to the BCCE from Equation (9).

With the formulation of the generalized brightness change constraint Equation (11) it is now possible to estimate reliable optical flow in applications where the BCCE failed due to its limitations.

5 OPTICAL FLOW OF TAYLOR DISPERSION

The projected intensity structure is given by

$$I = \sqrt{\left\| b^2 + \frac{2\cdot(c+x)}{a\cdot t} \right\|} - \sqrt{\left\| b^2 + \frac{2\cdot x}{a\cdot t} \right\|}. \tag{13}$$

This structure can be developed in a Taylor series around $t = 0$. This results in

$$I = \sqrt{\frac{2}{t}} \left(\sqrt{\frac{c+x}{a}} - \sqrt{\frac{x}{a}} \right) + \frac{b^2\sqrt{t}}{2\sqrt{2}} \left(\sqrt{\frac{a}{c+x}} - \sqrt{\frac{a}{x}} \right) + O\left(t^{3/2}\right). \tag{14}$$

Differentiating the first term of the expansion in time leads to

$$\frac{dI}{dt} = \frac{d}{dt} \left(\sqrt{\frac{2}{t}} \left(\sqrt{\frac{c+x}{a}} - \sqrt{\frac{x}{a}} \right) \right) = -\frac{1}{2t} I. \tag{15}$$

Estimating the velocity of the intensity structures subject to Taylor dispersion can thus be computed by solving the differential equation $dI/dt = -(2t)^{-1} I$. The isotropic diffusion process, which is also present in our application, this differential equation can be expanded to

$$\frac{dI}{dt} = u\frac{\partial I}{\partial x} + v\frac{\partial I}{\partial y} + \frac{\partial I}{\partial t} = D\Delta I - \frac{1}{2t} I. \tag{16}$$

This type of equation can be solved straight forward with the local gradient based approach presented in section 4. Rewriting this equation in vector notation leads to

$$\frac{dI}{dt} = d^\top \cdot p = \begin{pmatrix} \frac{\partial^2 I}{\partial x^2} + \frac{\partial^2 I}{\partial y^2} & \frac{1}{2t} I & \frac{\partial I}{\partial x} & \frac{\partial I}{\partial y} & \frac{\partial I}{\partial t} \end{pmatrix} \cdot \begin{pmatrix} -D & 1 & u & v & 1 \end{pmatrix}^\top = 0 \tag{17}$$

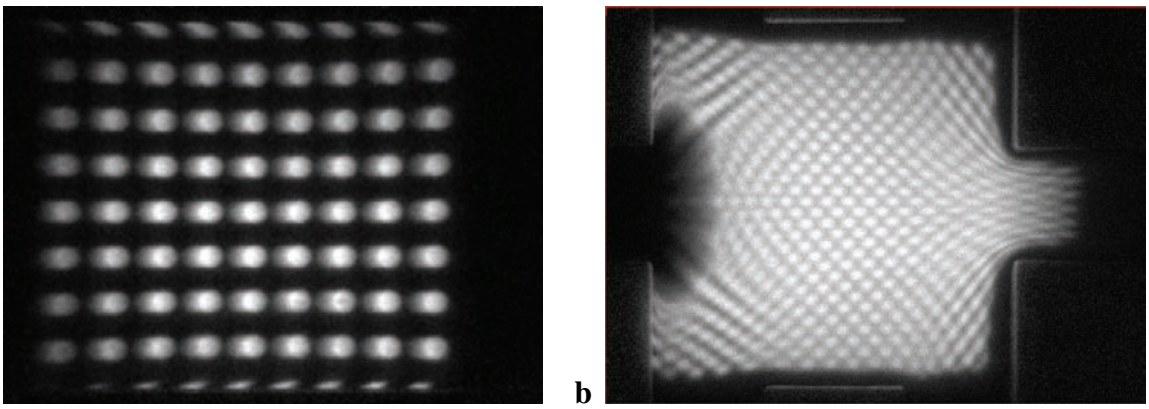

Fig. 3 A typical pattern written into a very simple microfluidic flow for calibration purposes in **a** and a little more interesting inhomogeneous flow in **b** .

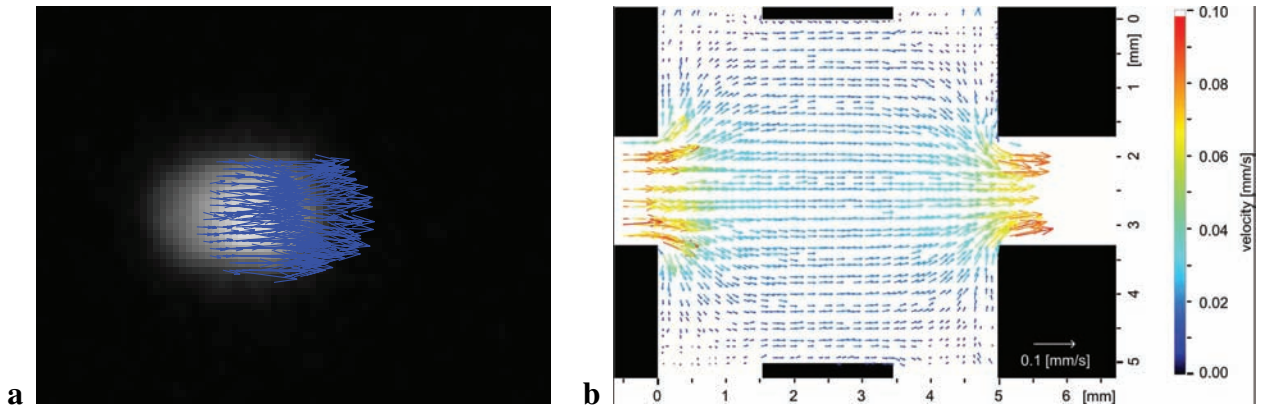

Fig. 4 Zoomed in view of the vector field around one of the dots written to the fluid is shown in **a** and the mean vector field of the mixing chamber.

This equation can then be solved by the algorithm detailed in [6]. Basically, the ill posed problem of Equation (17) is tackled by assuming that the parameter vector is the same in a local neighborhood. Equation (17) is thus written for each pixel in said neighborhood weighted by a Gaussian. This overdetermined system of equation can then be solved in a Total Least Squares (TLS) sense [20]. This boils down to a singular value analysis.

6 RESULTS

Through a range of measurements the pattern written with the masked laser into the fluid was optimized for the optical flow based algorithm presented in this contribution. Typical visualizations of two different microfluidic flows are presented in Figure 3. The flow field is computed from these image sequences. A zoomed in view of the flow field estimated at one of the point is shown in Figure 4**a** . The mean flow field estimated for the flow geometry shown in Figure 3**b** is presented in Figure 4**b** .

In order to test the accuracy of the algorithm, precisely known, homogeneous fluid flows were set up. Through knowledge of the fluid flow "'ground truth"' was acquired. The comparison of ground truth versus measured values is shown in Figure 5. The error bars in this plot result from five independent measurements.

From the test of ground truth to measured values it become apparent that the novel technique of measuring microfluidic flows exhibits excellent agreement. The ground truth values are within the error bars for all measured flow velocities.

7 CONCLUSION

In this contribution, an optical flow based technique for measuring microfluidic flows based on molecular tagging was presented. An extension to the brightness change constraint equation was derived, that allows to accurately estimate motion in the presence of Taylor dispersion. The novel algorithm was tested on ground truth sequences and showed excellent agreement. The algorithm was

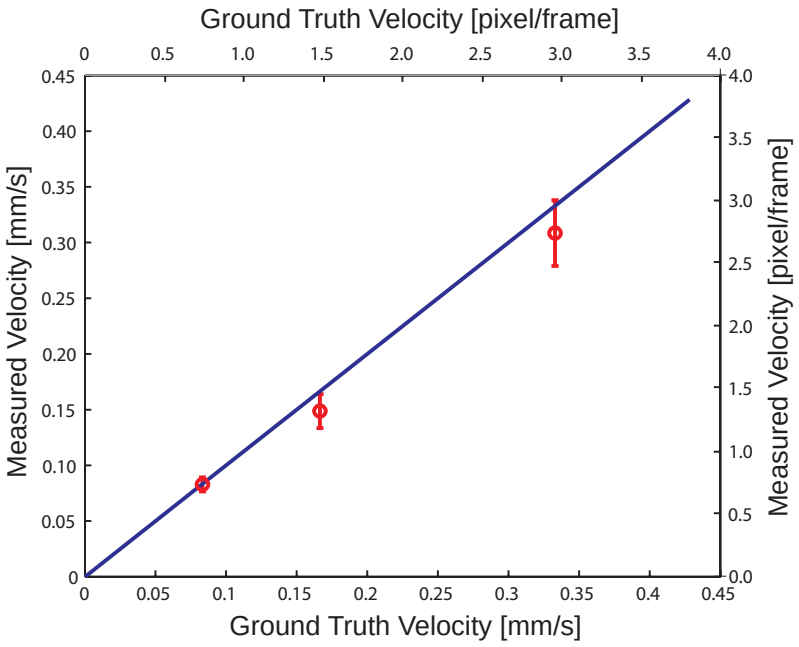

Fig. 5 Comparison of measured values compared to ground truth measurement. Error bars were computed from independent measurements.

also applied to inhomogeneous fluid flows in the mixing chamber and proved its applicability for this type of measurement.

The next step will be to compare measurement results of this technique to μPIV measurements conducted in the same chamber. The technique will then be applied to more challenging flows in the mixing chamber.

8 ACKNOWLEDGEMENT

The authors thank the German Research Foundation (Deutsche Forschungsgemeinschaft DFG) for funding this work in the framework of the DFG priority program SPP 1147.

REFERENCES

[1] M. Avram, A. Avram, and C. Iliescu. Biodynamical analysis microfluidic system. *Microelectronic Engineering*, 83(4-9):1688–1691, 2006.

[2] J. R. Burns and C. Ramshaw. The intensification of rapid reactions in multiphase systems using slug flow in capillaries. *Lab on a Chip*, 1(1):10–15, 2001.

[3] J. C. T. Eijkel and A. van den Berg. Nanofluidics: what is it and what can we expect from it? *Microfluidics and Nanofluidics*, 1(3):249–267, 2005.

[4] C. Fennema and W. Thompson. Velocity determination in scenes containing several moving objects. *Computer Graphics and Image Processing*, 9:301–315, 1979.

[5] C. S. Garbe and B. Jähne. Reliable estimates of the sea surface heat flux from image sequences. In *Proc. of the 23rd DAGM Symposium*, Lecture Notes in Computer Science, LNCS 2191, pp. 194–201. Springer-Verlag, Munich, Germany, 2001.

[6] C. S. Garbe, H. Spies, and B. Jähne. Estimation of surface flow and net heat flux from infrared image sequences. *Journal of Mathematical Imaging and Vision*, 19(3):159–174, 2003.

[7] C. S. Garbe, H. Spies, and B. Jähne. Mixed OLS-TLS for the estimation of Dynamic Processes with a Linear Source Term. In L. Van Gool, ed., *Pattern Recognition*, vol. LNCS 2449 of *Lecture Notes in Computer Science*, pp. 463–471. Springer-Verlag, Zurich, CH, 2002.

[8] H. Haußecker and D. J. Fleet. Computing Optical Flow with Physical Models of Brightness Variation. In *CVPR'00*, vol. 2, 2000.

[9] H. Haußecker and D. J. Fleet. Computing Optical Flow with Physical Models of Brightness Variation. *PAMI*, 23(6):661–673, June 2001.

[10] H. Haußecker, C. Garbe, H. Spies, and B. Jähne. A Total Least Squares for Low-Level Analysis of Dynamic Scenes and Processes. In *DAGM*, pp. 240–249. Springer, Bonn, Germany, 1999.

[11] B. K. P. Horn and B. Schunk. Determining Optical Flow. *Artificial Intelligence*, 17:185–204, 1981.

[12] P. K. Kundu. *Fluid Mechanics*. Academic Press, San Diego, CA, 1990.

[13] S. Negahdaripour. Revised Definition of Optical Flow: Integration of Radiometric and Geometric Cues for Dynamic Scene Analysis. *PAMI*, 20(9):961–979, September 1998.

[14] S. Negahdaripour and C. H. Yu. A Generalized Brightness Chane Model for Computing Optical Flow. In *International Conference in Computer Vision*, pp. 2–7. Berlin, 1993.

[15] N.-T. Nguyen and S. T. Wereley. *Fundamentals And Applications of Microfluidics, Second Edition*. Artech House Publishers, 2006.

[16] K. Roetmann, C. S. Garbe, W. Schmunk, and V. Beushausen. Micro-Flow Analysis by Molecular Tagging Velocimetry and Planar Raman-Scattering. In *Proc. of 12th International Symposium on Flow Visualization*, 2006.

[17] B. Schunk. The Image Flow Constraint Equation. *Computer Vision, Graphics and Image Processing*, 35:20–46, 1986.

[18] D. Sinton. Microscale flow visualization. *Microfluidics and Nanofluidics*, 1(1):2–21, 2004.

[19] G. Taylor. Conditions under which dispersion of a solute in a stream of solvent can be used to measure molecular diffusion. *Proc.Royal Soc.London Ser.A*, 225:473–477, 1954.

[20] S. Van Huffel and J. Vandewalle. *The Total Least Squares Problem: Computational Aspects and Analysis*. Society for Industrial and Applied Mathematics, Philadelphia, 1991.

[21] A. Verri and T. Poggio. Motion field and optical flow: Qualitative Properties. *IEEE Transactions on Pattern Analysis and Machine Intelligence*, 11(5):490–498, 1989.

[22] J. Wang. From DNA biosensors to gene chips. *Nucleic Acids Res.*, 28(16):3011–3016, 2000.

[23] D. Zhang and M. Herbert. Harmonic Maps and Their Applications in Surface Matching. In *CVPR'99*. Fort Collins, Colorado, June 1999.